Eur. Phys. J. D **36**, 123–128 (2005)
DOI: 10.1140/epjd/e2005-00174-9

THE EUROPEAN PHYSICAL JOURNAL D

Generation and decoherence of mesoscopic superposition states in a strongly driven micromaser

F. Casagrande[a] and A. Lulli

INFM, Dipartimento di Fisica, Università di Milano, Via Celoria 16, 20133 Milano, Italy

Received 15 March 2005 / Received in final form 10 May 2005
Published online 28 June 2005 –

Abstract. We show that the decoherence of mesoscopic superposition states of a cavity field can be observed when an additional classical field strongly drives the atoms in a micromaser like device. Due to solvable system dynamics, analytical expressions provide phase space descriptions of all stages of atom pair correlation measurements at steady-state in the presence of pumping, driving, and dissipative effects. The detection of the first atom prepares a pure field state, which entangles with the second atom that acts as a meter. The decoherence rate, derived from conditional probabilities for atomic detection, depends on the square of the interaction time, that is the parameter that rules the separation in phase space between the pure state components. The quantum coherence is unaffected by the atomic pumping. Starting instead the correlation measurement from a vacuum state and without pumping the cavity we propose an alternative method to monitor the decoherence of Schrödinger cat states.

PACS. 42.50.Pq Cavity quantum electrodynamics; micromasers – 03.65.Yz Decoherence; open systems; quantum statistical methods

1 Introduction

The interaction of a quantum system with the environment or a measuring apparatus destroys the quantum coherence of a pure state. This decoherence process makes the extraordinary richness of the state space inaccessible to the macroscopic world, making studies of decoherence of the outmost relevance for an understanding of the boundary between the microscopic and the macroscopic domains [1]. Furthermore, progress in quantum information and the implementation of quantum gates for computational purposes requires an exquisite coherence control, making decoherence a central issue also in a more pragmatic approach [2].

Among the many relevant frameworks for these investigations, we consider cavity quantum electrodynamics (CQED) [3], where atoms and photons can be entangled with a superb experimental accuracy [4] and the system dynamics described by relatively simple models. Precisely in CQED a remarkable experiment [5] showed the generation and monitored the decoherence of superpositions of two coherent states of the cavity field with the same amplitude but opposite phases, examples of the so-called Schrödinger cat states whose components are separated in phase space by a mesoscopic distance [6]. Similar results were found in the motional atomic states of a trapped ion [7].

[a] e-mail: federico.casagrande@mi.infn.it

We recently investigated a system, the strongly driven micromaser (SDM) [8], that is a micromaser [9], another achievement in CQED, where a classical resonant field is added to strongly drive the atoms only when they cross the cavity. The SDM exemplifies the above mentioned features of CQED: it is exactly solvable, and its implementation appears quite feasible. In [8] we investigated both the lossless unitary dynamics at the basis of the SDM [10], and the open system dynamics, deriving closed expressions for all relevant time dependent and stationary physical quantities, including two atom correlation functions that exhibit quantum correlations mediated by the cavity field.

In this paper, starting from a new formulation of the main results of [8], we investigate the cavity field structures created in the steady-state regime of an SDM. By calculations based on the quantum characteristic function we describe the generation and the decoherence of mesoscopic superposition states of the cavity field in an SDM. The decoherence can be observed by atom-pair correlation measurements at steady-state, i.e., in the presence of pumping, driving, and dissipative effects. The detection of the first probe atom prepares a pure state of the cavity field, which entangles with the second atom that acts as a meter. The decoherence rate of mesoscopic superpositions scales as the squared atomic transit time, that is the parameter that rules the separation in phase space between the components of the superposition. Decoherence can be monitored by atomic conditional probabilities that

turn out to be independent of the atomic pumping rate. In fact, the coherence properties of the pure states are not affected by the atomic pumping.

On the other hand, if the first atom of the pair enters the cavity prepared in the vacuum state, the superposition states generated by its detection are Schrödinger cats. In the absence of atomic pumping, their decoherence can be described and monitored by the same correlation measurements as above, and the decoherence rate is the same as for steady-state operation. In comparison with the method of [5], the interaction is resonant rather than dispersive, and the atoms are not manipulated before or after the cavity, but are coherently driven inside.

In Section 2 we introduce all relevant results on the dynamics of a strongly driven micromaser. In Section 3 we describe the generation and decoherence of mesoscopic superposition states of the cavity field. In Section 4 we show how the scheme can be adapted to describe the decoherence of cat states. Concluding remarks are reported in Section 5.

2 Strongly driven micromaser dynamics

In a micromaser [9] a Poissonian beam of two-level atoms, selected in velocity and excited to Rydberg levels, is injected at a rate r in a high-Q superconductive microwave cavity where one mode is resonant with an atomic transition between states $|e\rangle$ and $|g\rangle$. At most one atom is present in the cavity: $t_{int} \ll r^{-1} \ll \gamma^{-1}$, where t_{int} is the interaction time, γ^{-1} the cavity photon lifetime, and the decay of atomic levels is quite negligible. In an SDM the atoms are also strongly driven, only inside the cavity, by a transverse classical field that is uncoupled to the cavity mode. The single atom interaction can be described by the following Hamiltonian [8,10], in the interaction picture and rotating wave approximation:

$$\hat{H} = \frac{\hbar g}{2}(\hat{\sigma}^\dagger + \hat{\sigma})(\hat{a}^\dagger + \hat{a}), \tag{1}$$

where $\hat{a}$ ($\hat{a}^\dagger$) is the field annihilation (creation) operator, and $\hat{\sigma} = |g\rangle\langle e|$ ($\hat{\sigma}^\dagger = |e\rangle\langle g|$) the atomic lowering (raising) operator, and g is the coupling frequency (taken real for simplicity). When an excited atom enters the cavity, the initial system density operator $\rho_0 = \rho_{F,0} \otimes |e\rangle\langle e|$ undergoes a unitary evolution:

$$\rho_0 \to \rho_1 = \hat{U}(\xi)\rho_0\hat{U}(-\xi) \tag{2}$$

where

$$\begin{aligned}\hat{U}(\xi) &= \hat{D}(\xi)|+\rangle\langle +| + \hat{D}(-\xi)|-\rangle\langle -| \\ &= \hat{C}_e(\xi)\hat{I}_A - i\hat{C}_g(\xi)\hat{\sigma}_x\,.\end{aligned} \tag{3}$$

In equation (3) $\hat{D}(\xi) = \exp(\xi\hat{a}^\dagger - \xi^*\hat{a})$ is the displacement operator where the parameter $\xi = -igt_{int}/2$. Note that the strength of the classical driving field does not appear due to the strongly driven approximation [10]. The system dynamics consists in cavity field displacements along the imaginary axis correlated with the atomic states $|\pm\rangle = (1/\sqrt{2})(|g\rangle \pm |e\rangle)$, that are the eigenstates of $\hat{\sigma}_x$, i.e., a different entanglement than the usual Jaynes-Cummings interaction and Rabi oscillations [11]. It proves quite useful to introduce the operators $\hat{C}_{e,g}(\xi)$ describing the cavity field evolution when the atom does not change its state, or changes it, respectively, in the basis $\{|e\rangle, |g\rangle\}$:

$$\begin{aligned}\hat{C}_e(\xi) &= [\hat{D}(\xi) + \hat{D}(-\xi)]/2 \\ \hat{C}_g(\xi) &= i[\hat{D}(\xi) - \hat{D}(-\xi)]/2.\end{aligned} \tag{4}$$

These operators are hermitian and commuting measurement operators [2] for the cavity field, that obey the sum rule: $\hat{C}_e^2(\xi) + \hat{C}_g^2(\xi) = \hat{I}_F$. Actually, from equations (2–4) it follows that when the atom leaving the cavity is not observed, the field density operator evolution is:

$$\rho_{F,0} \to \rho_{F,1} = \mathrm{Tr}_A\rho_1 = \hat{C}_e\rho_{F,0}\hat{C}_e + \hat{C}_g\rho_{F,0}\hat{C}_g \tag{5}$$

where Tr_A is the partial trace over a basis in the atomic Hilbert space. By combining the unitary dynamics (5) with the incoherent one due to a weak coupling to the environment, that introduces dissipation and thermal fluctuations, and by taking pumping into account, we can write the master equation for $\rho_F(t)$ [8], that we present here in the Lindblad form and for dimensionless time ($\gamma t \equiv t$ from now on):

$$\dot{\rho}_F(t) = \sum_{m=1}^{4}\left[\hat{C}_m\rho_F(t)\hat{C}_m^\dagger - \frac{1}{2}\left(\hat{C}_m\hat{C}_m^\dagger\rho_F(t) + \rho_F(t)\hat{C}_m^\dagger\hat{C}_m\right)\right] \tag{6}$$

where $\hat{C}_{1,2} = \sqrt{N_{ex}}\hat{C}_{e,g}$, $\hat{C}_3 = \sqrt{\bar{n}+1}\hat{a}$, $\hat{C}_4 = \sqrt{\bar{n}}\hat{a}^\dagger$, $N_{ex} = r/\gamma$ is a dimensionless pumping rate and $\bar{n}$ the mean thermal photon number. By well known techniques [12] the master equation (6) can be mapped into a partial differential equation for the quantum characteristic function $\chi(\alpha,t) = \mathrm{Tr}_F\left\{\rho_F(t)\hat{D}(\alpha)\right\}$:

$$\begin{aligned}\frac{\partial}{\partial t}\chi(\alpha,\alpha^*,t) = &\left[\frac{N_{ex}}{2}\left(e^{\xi^*\alpha - \xi\alpha^*} + e^{-\xi^*\alpha + \xi\alpha^*} - 2\right)\right. \\ &\left. -\frac{1}{2}(2\bar{n}+1)|\alpha|^2\right]\chi(\alpha,\alpha^*,t) \\ &-\frac{1}{2}\left(\alpha\frac{\partial}{\partial\alpha} + \alpha^*\frac{\partial}{\partial\alpha^*}\right)\chi(\alpha,\alpha^*,t)\end{aligned} \tag{7}$$

whose solution is [8]:

$$\chi(\alpha,t) = \frac{\chi^{SS}(\alpha)\chi_0(\alpha e^{-\frac{t}{2}})}{\chi^{SS}(\alpha e^{-\frac{t}{2}})} \tag{8}$$

where $\alpha \equiv (\mathrm{Re}\alpha, \mathrm{Im}\alpha)$, χ_0 is the characteristic function of the initial state $\rho_{F,0}$, and the steady-state distribution

can be written as:

$$\chi^{SS}(\alpha) = \exp\left[-(\bar{n}+\tfrac{1}{2})|\alpha|^2 - 2N_{ex}\int_0^{2|\xi|Re\alpha}\frac{1-\cos(z)}{z}dz\right]$$
$$= \exp\left[-(\bar{n}+\tfrac{1}{2})|\alpha|^2 + N_{ex}\sum_{n=1}^{\infty}\frac{(-1)^n(2|\xi|\mathrm{Re}\alpha)^{2n}}{n(2n)!}\right]. \quad (9)$$

The steady state, as investigated in [8], is a super-Poissonian field with coherence and phase properties, at variance with the micromaser field that alternates between sub- and super-Poissonian photon statistics and is purely diagonal in the Fock basis. The field amplitude expectation value vanishes but the mean photon number can be large: $\langle\hat{a}^\dagger\hat{a}\rangle^{SS} = N_{ex}|\xi|^2 + \bar{n}$.

3 Generation and decoherence of mesoscopic superposition states

Now let us focus on atomic correlation measurements when the system is at steady-state. The measurement of one outgoing atom prepares the cavity field in one of the two states

$$\rho_{F,1}^{(e),(g)} = \frac{\hat{C}_{e,g}\rho_F^{SS}\hat{C}_{e,g}}{p_{e,g}} \quad (10)$$

where $p_{e,g}$ is the probability for the atom to be measured in the upper (lower) state:

$$p_{e,g} = \mathrm{Tr}_F\{\hat{C}_{e,g}^2\rho_F^{SS}\} = [1 \pm \chi^{SS}(2\xi)]/2, \quad (11)$$

where $\chi^{SS}(2\xi) = \exp\{-4(\bar{n}+1/2)|\xi|^2\}$. Hence the probabilities (11) are independent of the atomic pumping rate N_{ex}. This is quite different than in a standard micromaser, where the atomic probabilities $p_{e,g}$ depend on N_{ex} via the steady-state photon statistics [13].

The states of (10) are described in phase space by the characteristic functions:

$$\chi_1^{(e),(g)}(\alpha) = \mathrm{Tr}_F\{\rho_{F,1}^{(e),(g)}\hat{D}(\alpha)\}$$
$$= \frac{\cos(2|\xi|\mathrm{Re}\alpha)\chi^{SS}(\alpha) \pm [\chi^{SS}(\alpha+2\xi)+\chi^{SS}(\alpha-2\xi)]/2}{1\pm\chi^{SS}(2\xi)}$$
$$= \chi^{SS}(\alpha)\frac{\cos(2|\xi|\mathrm{Re}\alpha) \pm \chi^{SS}(2\xi)\cosh[2|\xi|(1+2\bar{n})\mathrm{Im}\alpha]}{1\pm\chi^{SS}(2\xi)}. \quad (12)$$

In the derivation of (12) we used the properties of trace and the operator relation: $\hat{C}_{e,g}\hat{D}(\alpha)\hat{C}_{e,g} = \cos(2|\xi|\mathrm{Re}\alpha)\hat{D}(\alpha) \pm [\hat{D}(\alpha+2\xi)+\hat{D}(\alpha-2\xi)]/2$. This relation is the key for understanding the generation of a tripartite structure in phase space, as it is the case of the function $\chi_1^{(e)}(\alpha)$ shown in Figure 1 for a set of realistic parameters, $|\xi| = \pi$, $N_{ex} = 10$ and $\bar{n} = 0.03$. The interference effects due to quantum coherence show up in the lateral structures of the characteristic function; the central part alone would describe the cavity field state if the atom were not observed, i.e., $\rho_{F,1} = p_e\rho_{F,1}^{(e)} + p_g\rho_{F,1}^{(g)}$.

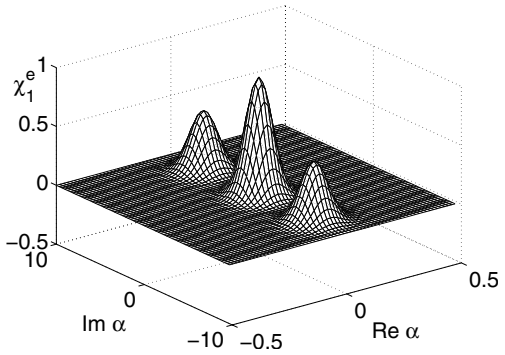

Fig. 1. Quantum characteristic function $\chi_1^{(e)}(\alpha)$ of the steady state cavity field after the measurement of a probe atom in the excited state, see equation (12), for displacement parameter $|\xi| = \pi$, pumping rate $N_{ex} = 10$ and mean thermal photon number $\bar{n} = 0.03$.

The section along the imaginary axis, that is independent of atomic pumping rate N_{ex}, consists in three peaks centered at $0, \pm 2\xi$, whose heights are $1, 1/2$, respectively. These peaks are well separated for $|\xi| \gtrsim 2$, i.e., $g \gtrsim t_{int}^{-1}$, easily verified in the strong coupling regime where $g \gg \gamma^{-1}, \gamma_a^{-1}$. In this case the superposition state components are mesoscopically separated in phase space. As for the modulation of the central part along the real axis, expected from (12), it is not evident just because the whole distribution is severely reduced in its dependence on the variable $\mathrm{Re}\alpha$ due to the peculiar shape of $\chi^{SS}(\alpha)$. This effect is due to the series expansion in (9), that originates from the interaction with the atoms, and that produces a truncation in $\mathrm{Re}\alpha$.

Now we let the states (12) evolve according to the master equation (6) for a dimensionless time interval τ, where (by using (8)):

$$\chi_1^{(e),(g)}(\alpha,\tau) = \frac{\chi^{SS}(\alpha)}{1\pm\chi^{SS}(2\xi)}\{\cos(2|\xi|\mathrm{Re}\alpha e^{-\tau/2})$$
$$\pm \chi^{SS}(2\xi)\cosh[2|\xi|(1+2\bar{n})\mathrm{Im}\alpha e^{-\tau/2}]\}. \quad (13)$$

As an example, starting from $\chi_1^{(e)}(\alpha,0)$ of Figure 1, we obtain the function $\chi_1^{(e)}(\alpha,\tau)$ shown in Figure 2 for a time $\tau = 0.05$, i.e. $\tau \ll 1$ so that the dissipative effects are negligible, and $\tau \ll N_{ex}^{-1}$, so that the effects of the pumping atoms are reduced. It is remarkable that, after only one twentieth of the photon lifetime the lateral structures that are the signature of quantum coherence appear so strongly reduced.

After the time τ, we can measure a second probe atom outgoing from the cavity, where it was entangled with the field state (13) prepared by the measurement of the first probe atom and the interaction of nearly N_{ex} unmeasured pumping atoms. Hence, we consider a set of measurements for atom pairs separated by a time interval τ, whose outcomes can be compared with the conditional probabilities for the observation of the second atom in the upper or

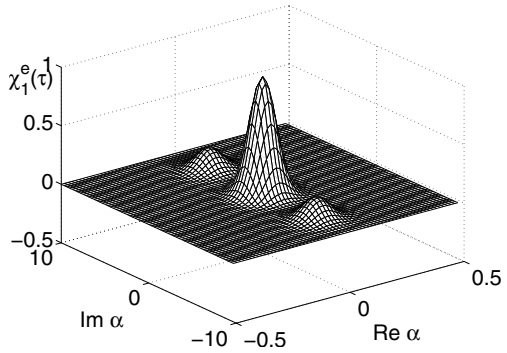

Fig. 2. Time dependent quantum characteristic function $\chi_1^{(e)}(\alpha,\tau)$ from equation (13), evolved from $\chi_1^{(e)}(\alpha,0)$ of Figure 1 at $\tau = 0.05$.

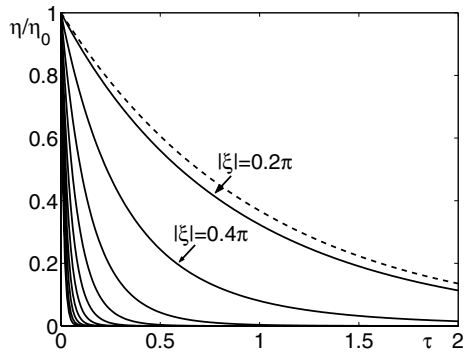

Fig. 3. Solid lines: normalized decoherence signal (16) vs. dimensionless time τ, for $\bar{n} = 0.03$, and $|\xi|/\pi = 0.2, 0.4, ..., 2$. Dashed line: dissipative exponential decay.

lower state, given the detection of the first one in either state. The expressions of these conditional probabilities are simply related to the characteristic functions (13):

$$P_{(e/e),(g/e)}(\tau) = \mathrm{Tr}_F\{\hat{C}^2_{e,g}\rho^{(e)}_{F,1}(\tau)\} = [1 \pm \chi_1^{(e)}(2\xi,\tau)]/2$$
$$P_{(e/g),(g/g)}(\tau) = \mathrm{Tr}_F\{\hat{C}^2_{e,g}\rho^{(g)}_{F,1}(\tau)\} = [1 \pm \chi_1^{(g)}(2\xi,\tau)]/2. \quad (14)$$

Since all conditional probabilities (14) depend on the functions (13) evaluated for imaginary arguments ($2\xi = -igt_{int}$), they are independent of the atomic pumping rate N_{ex}, like the one-atom probabilities (11). Also we remark that the joint probabilities for atom pair detections in different states are equal, $W_{eg}(\tau) = W_{ge}(\tau)$; i.e., these two sequences of unobserved atoms leave the cavity in the same state, which gives rise to interference effects in the SDM. All these features of the atomic correlations in an SDM are not exhibited by the atomic correlations in a standard micromaser [14].

Now, in order to monitor the decoherence, following [5] we consider the decoherence signal

$$\eta(\tau) \equiv P_{(e/e)}(\tau) - P_{(e/g)}(\tau). \quad (15)$$

From (14) and (15) we obtain

$$\frac{\eta(\tau)}{\eta(0)} = \frac{\cosh[4(1+2\bar{n})|\xi|^2 e^{-\tau/2}] - 1}{\cosh[4(1+2\bar{n})|\xi|^2] - 1}. \quad (16)$$

In the limit $2|\xi|^2 \ll 1$, that is for very short interaction times, we find an exponential decay

$$\eta(\tau) \simeq \eta(0)e^{-\tau}. \quad (17)$$

In this case the components of the cavity field superposition states (12) are not resolved in phase space, hence decoherence effects are expected to be negligible; both states simply relax to steady-state due to the dissipative coupling to the environment, which shows up in the exponential decay of $\eta(\tau)$. In the opposite limit of long interaction times, $2|\xi|^2 \gg 1$, and for short delay times, $\tau \ll 1$, from equation (16)

$$\eta(\tau) \simeq \eta(0)e^{-2(1+2\bar{n})|\xi|^2\tau}, \quad (18)$$

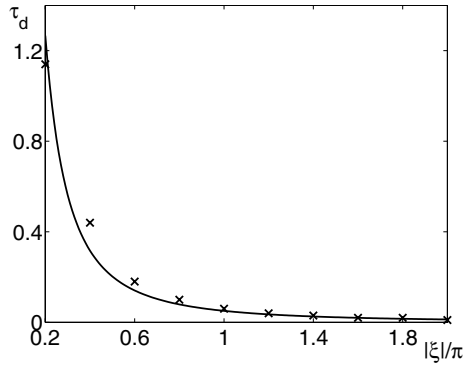

Fig. 4. Crosses: dimensionless decoherence time τ_D for all values of $|\xi|$ in Figure 3. Solid line: curve $\tau_D = (2|\xi|^2)^{-1}$.

where $\eta(0) = 2p_e p_g \simeq 1/2$, because $p_{e,g} \simeq 1/2$. Again we find an exponential decay, but it is much faster than the dissipative one: the rate is, for negligible thermal effects ($\bar{n} \ll 1$), $\gamma_D = 2|\xi|^2 \gg 1$. In this case the cavity field is prepared in superposition states whose components are separated in phase space by a mesoscopic distance. Hence the system is expected to exhibit a truly decoherent dynamics, in which the pure states reduce to a statistical mixture much before their relaxation to steady-state. This leads to the behaviour described by (18). In Figure 3 we show the behavior of $\eta(\tau)/\eta(0)$ for several values of the displacement parameter $|\xi|$, and we compare with the exponential dissipative decay of the mean photon number, $\langle\hat{a}^\dagger\hat{a}\rangle(\tau)/\langle\hat{a}^\dagger\hat{a}\rangle(0) = e^{-\tau}$. By increasing the parameter $|\xi|$, that is proportional to the interaction time, we see the transition from dissipative to decoherent dynamics, as described by (17) and (18), respectively. We observe that the dimensionless decoherence time τ_D, corresponding to $\eta(\tau_D)/\eta(0) = e^{-1}$ in Figure 3, for $|\xi| \geq \pi$ scales as the inverse number of quanta in the field state, i.e., as the squared distance in phase space, in agreement with the predictions of decoherence theories [1,6]. In Figure 4 we show $\eta(\tau_D)$ as a function of the parameter $|\xi|$, together with the curve $\tau_D = (2|\xi|^2)^{-1}$.

We notice that the atomic pumping does not play any role in the decoherence process. In fact, equation (13) shows that the dynamics of the coherence properties of the

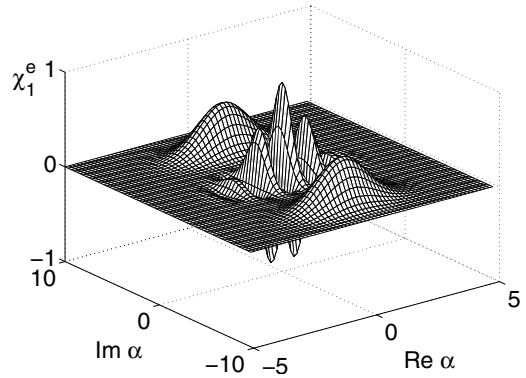

Fig. 5. Cat state: quantum characteristic function $\chi_1^{(e)}(\alpha)$ after the measurement of the first probe atom in the excited state, see equation (12), starting from the thermal state approaching the vacuum state ($\bar{n} = 0.03$), and for displacement parameter $|\xi| = \pi$.

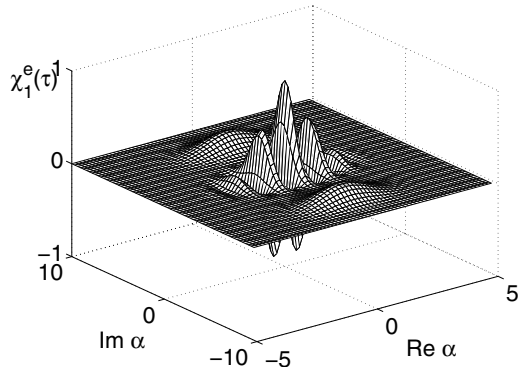

Fig. 6. Time dependent quantum characteristic function $\chi_1^{(e)}(\alpha, \tau)$ from equation (13), evolved from the cat state $\chi_1^{(e)}(\alpha, 0)$ of Figure 5 at $\tau = 0.05$.

superposition states depends only on the imaginary part of the field amplitude. Hence coherence is protected from the effect of the atomic pumping, that on the contrary affects the dependence of the state only on the real part (see the master Eq. (7) and its solution (8), (9)). Hence atomic pumping does not add to dissipation in accelerating the decoherence.

4 Generation and decoherence of mesoscopic cat states

Now we consider atomic correlations starting from the cavity in a thermal state instead of the SDM steady-state, and in the absence of a flux of pumping atoms. This state is described in phase space by the characteristic function $\chi_0(\alpha) = \exp[-(\bar{n} + 1/2)|\alpha|^2]$. According to our scheme, we inject a first probe atom that is strongly driven during its transit in the cavity. The detection of this atom in the upper (lower) state generates a state that is described in phase space by the quantum characteristic function:

$$\chi_1^{(e),(g)}(\alpha) = \chi_0(\alpha)\frac{\cos(2|\xi|\mathrm{Re}\alpha) \pm \chi_0(2\xi)\cosh[2|\xi|(1+2\bar{n})\mathrm{Im}\alpha]}{1 \pm \chi_0(2\xi)}. \tag{19}$$

In the ideal case of $\bar{n} = 0$ we have an even or odd cat state of the cavity field of the following form, respectively: $|\psi\rangle_1^{(e),(g)} \propto (|\xi\rangle \pm |-\xi\rangle)$. This is due to the underlying system Hamiltonian [10], containing both Jaynes-Cummings and anti-JC terms, formally the same as for a trapped ion in the Lamb-Dicke regime [15]. As an example, in Figure 5 we show the characteristic function $\chi_1^{(e)}(\alpha)$ thus obtained. In Figure 6 we see that, after a dimensionless time $\tau = 0.05$, the coherences of the cat state of Figure 5 are drastically reduced, just as in Figure 2 compared with Figure 1 for steady-state operation. In fact, we can still apply the treatment of the previous section also to describe and monitor the decoherence of mesoscopic cat states. Again we inject a second atom through the cavity, after a short time interval τ in which the cavity field simply undergoes a dissipative decay towards the steady-state, that now coincides with the initial thermal state (see (9) for $N_{ex} = 0$). After the detection of the second atom, the system must be reset to the initial condition, and then the procedure must be repeated until a reliable statistics of the atomic correlations is obtained. By our treatment with $N_{ex} = 0$ and $\chi^{SS}(\alpha) = \chi_0(\alpha)$, we exactly recover the conditional probabilities (14) and the decoherent behaviour (18) for mesoscopic extension of the cat states, as in the general case of steady-state operation with atomic pumping. This agrees with the previous remarks on the independence of decoherence from the pumping rate, that is exactly zero in this case.

5 Conclusion

In summary, we considered a strongly driven micromaser, that is an open quantum system that is exactly solvable and can be experimentally implemented. In particular, we have shown that, by adding a classical field that drives the atoms in the cavity of a standard micromaser set-up, atomic correlation measurements at steady-state can allow observing the decoherence of mesoscopic superposition states of the cavity field, induced by the coupling to the environment. The ratio of decoherent to dissipative decay rate turns out to scale as the squared interaction time: $\gamma_D/\gamma = (gt_{int})^2/2$. Our analysis also shows that decoherence is independent of the atomic pumping rate. Hence our treatment suggests a method to investigate the boundary between the quantum and the classical world in an open quantum system with a full interplay among driving, pumping, and dissipative effects.

On the other hand, starting from the vacuum state and in the absence of an atomic beam that pumps the cavity, the same conditional probabilities calculated at steady-state describe the decoherence of Schrödinger cat states,

just as it can be observed when the first atom of the correlated pairs finds the cavity in the vacuum state. In that case our method offers some new perspectives to the investigation of the decoherence of mesoscopic cat states in the microwave domain of cavity QED. In comparison with [5], our scheme is based on a resonant instead of dispersive atom-photons interaction; the atoms are strongly driven by a classical field in the cavity instead of being manipulated by classical pulses before and after the interaction; the phase difference between the two equal amplitude coherent states is π, which was not the case in the experiment.

These results can be relevant for applications in the preparation, control, and manipulation of quantum states for quantum information purposes.

References

1. E. Joos, H.D. Zeh, C. Kiefer, D. Giulini, J. Kupsch, I.-O. Stamatescu, *Decoherence and the Appearance of a Classical World in Quantum Theory* (Springer, Berlin, 2003); W.H. Zurek, Rev. Mod. Phys. **75**, 715 (2003)
2. M.A. Nielsen, I.L. Chuang, *Quantum Computation and Quantum Information* (Cambridge University Press, Cambridge, 2000)
3. H. Mabuchi, A.C. Doherty, Science **298**, 1372 (2002)
4. J.M. Raimond, M. Brune, S. Haroche, Rev. Mod. Phys. **73**, 565 (2001)
5. M. Brune, E. Hagley, J. Dreyer, X. Maitre, C. Wunderlich, J.-M. Raimond, S. Haroche, Phys. Rev. Lett. **77**, 4887 (1996)
6. A.O. Caldeira, A.J. Leggett, Phys. Rev. A **31**, 1059 (1985); D.F. Walls, G.J. Milburn, Phys. Rev. A **31**, 2403 (1985); B. Yurke, D. Stoler, Phys. Rev. Lett. **57**, 13 (1986); W. Schleich, M. Pernigo, F.L. Kien, Phys. Rev. A **44**, 2172 (1991); M. Brune, S. Haroche, J.M. Raimond, L. Davidovich, N. Zagury, Phys. Rev. A **45**, 5193 (1992)
7. C. Monroe, D.M. Meekhof, B.E. King, D.J. Wineland, Science **272**, 1131 (1996); C.J. Myatt, B.E. King, Q.A. Turchette, C.A. Sackett, D. Kielpinski, W.M. Itano, C. Monroe, D.J. Wineland, Nature **403**, 269 (2000)
8. P. Lougovski, F. Casagrande, A. Lulli, B.-G. Englert, E. Solano, H. Walther, Phys. Rev. A **69**, 023812 (2004)
9. D. Meschede, H. Walther, G. Müller, Phys. Rev. Lett. **54**, 551 (1985); G. Rempe, H. Walther, N. Klein, Phys. Rev. Lett. **58**, 353 (1987)
10. E. Solano, G.S. Agarwal, H. Walther, Phys. Rev. Lett. **90**, 027903 (2003)
11. E.T. Jaynes, F.W. Cummings, Proc. IEEE **51**, 89 (1963); H. Paul, Ann. Phys. **11**, 411 (1963)
12. K.E. Cahill, R.J. Glauber, Phys. Rev. **177**, 1882 (1969)
13. P. Filipowicz, J. Javanainen, P. Meystre, Phys. Rev. A **34**, 3077 (1986); L.A. Lugiato, M.O. Scully, H. Walther, Phys. Rev. A **36**, 740 (1987)
14. B.-G. Englert, M. Löffler, O. Benson, B. Varcoe, M. Weidinger, H. Walther, Fortschr. Phys. **46**, 897 (1998)
15. D. Leibfried, R. Blatt, C. Monroe, D. Wineland, Rev. Mod. Phys. **75**, 281 (2003)